Superresolved image reconstruction from incomplete data

Fiddy, Michael A.; Chuang, Yi-Chen; Dudley, Richard

2012

https://hdl.handle.net/10356/98853

https://doi.org/10.1117/12.930836

Superresolved Image Reconstruction from Incomplete Data

Yi-Chen Chuang[a], Richard Dudley[b], Michael A. Fiddy[c]

[a]School of Electrical and Electronic Engineering, Nanyang Technological University, 50 Nanyang Avenue, 639798, Singapore; [b]Department of Physics and Optical Science, University of North Carolina at Charlotte, 9201 University City Blvd, Charlotte, North Carolina 28223, USA; [c]Center for Optoelectronics and Optical Communications, University of North Carolina at Charlotte, 9201 University City Blvd, Charlotte, North Carolina 28223, USA

ABSTRACT

A finite thickness slab of a metamaterial having a refractive index close to $n = -1$, can be used for sub-wavelength scale imaging. In the image domain, the measured fields contain evanescent wave contributions from subwavelength scale features in the object but these have to be related to the intrinsic parameters describing the scatterer such as refractive index or permittivity. For weak scatterers there can be a simple relationship between the field distribution and the permittivity profile. However for strong (multiple) scatterers and, more importantly, for objects for which subwavelength features contribute to the scattered (near) field, there is no simple relationship between the measured data and the permittivity profile. This is a significant inverse scattering problem for which no immediate solution exists and given the metamaterial slab's limitations one cannot assume that either angle or wavelength diversity will be available to apply an inverse scattering algorithm. We consider wavelength diversity in this paper to acquire the measured data necessary to estimate a superresolved solution to the inverse scattering problem.

Keywords: Metamaterials, superresolution, scattering, inverse scattering algorithm

1. INTRODUCTION

Imaging normally involves a physical lens of some sort and the ultimate resolution is limited to its so-called diffraction limit, which depends on the wavelength used and the diameter of that lens, [1]. To achieve superresolution, or resolution either beyond the diffraction limit of the lens, or even beyond that of, say, $\lambda/4$, it is generally accepted that one must utilize an imaging system that captures near-field waves emerging from the object of interest. Avoiding the use of a lens and measuring the scattered field from an object all around that object (i.e. at all scattering angles for all incident illumination directions) still requires near field measurements to improve over $\sim \lambda/4$. The reason for this is well-known. Subwavelength scale features in an object scatter into evanescent waves that decay exponentially in the direction of propagation. They can couple back into propagating waves which only serves to complicate the eventual interpretation of the measured data. Much interest has been stirred in so-called perfect lenses. An ideal perfect $n=-1$ lens can successfully provide a superresolved field pattern in its image domain [2]. The object is placed in the near field of this lens and much effort has gone into trying to avoid having to also measure the image in the near field, e.g [3]. However, of interest to us here is recognizing that the measured field pattern might not take on the appearance of the permittivity profile or refractive index profile of the scattering object, which is what we expect when forming an image. In other words, what we measured is not necessarily easily interpreted into what the object looks like. For example, illuminating two slits in a penetrable dielectric medium and using a perfect lens, may give perfect fields in the image domain in the sense that this is the field pattern that emerged from the two slits, but it is not an image of the two slits. We make the point that as efforts are made to improve the performance of negative index materials in order to use them for this purpose, the interpretation of the images obtained can get increasingly complicated. Multiple scattering, especially of evanescent waves, leads to a field pattern in the image domain of the lens, that an inverse scattering algorithm must be applied to. Moreover, this inverse scattering algorithm can probably not rely on weak scattering approximations like the first Born approximation [4], in order to simplify their implementation, as resolution limits are push further. Our goal to figure out how the field in the image domain of a negative index lens relates to the permittivity profile of the scattering object, and how the usual requirements of multiple incident field directions or wavelengths needed for inverse scattering

algorithms, can be still be exploited. We say this since for the foreseeable future, negative index lenses made from metamaterials, are likely to be quite limited in both depth of focus and bandwidth, [5-8].

2. SYSTEM SETUP AND GENERAL OBSERVATIONS

In this study, two dielectric objects (permittivity, ε = 3.9, assumed constant for simplicity) are placed in front of a superlens slab ε_{lens}=-1-10^{-2}i (based on exp($+i\omega t$) convention) as shown in Figure 1 with dimensions indicated. A commercial software package, COMSOL (v.4.2a), based on finite element method, is used to obtain electric fields and time averaged electric energy density distributions. Periodic boundary conditions (top and bottom) and scattered boundary conditions (left and right) are assumed in the simulations. An incident TE-polarized ($E_x=E_y$=0; E_z=exp(-$i*k_0*x$)) plane wave is assigned in the simulations.
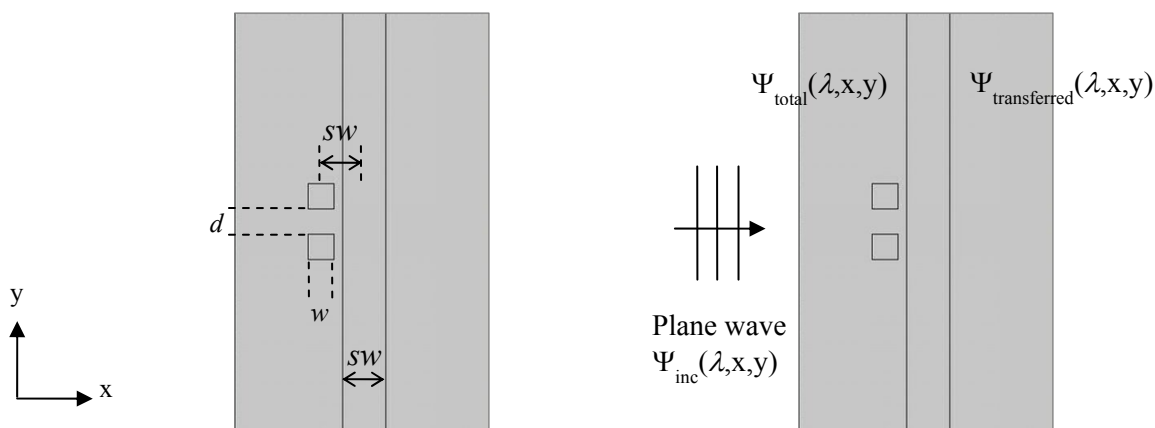

Figure 1. Geometry of the imaging system. Two square dielectric objects (ε=3.9) are placed in front of a metamaterial superlens (ε_{lens}= -1-10^{-2}i). The width of the blocks (w) is 240 nm; center-to-center distance between the blocks ($d+w$) is 480 nm; superlens width (sw) is 400 nm; center-to-center distance between the blocks and the superlens is also 400 nm. The incident plane wave (Ψ_{inc}) is TE polarized ($E_x=E_y$=0; E_z= exp(-$i*k_0*x$)). Ideally, the transferred field in the image domain ($\Psi_{transferred}$) should be identical to the total field (Ψ_{total}) in the object domain, where $\Psi_{total} \sim$ V(x,y)*Ψ_{inc}(λ,x,y) based on the first Born approximation.

An example is shown in Figure 2(a). It is important to notice that the total field on both sides of the lens and inside the lens is very complex. There are multiple interference patterns related to (i) the boundary conditions and (ii) evanescent waves propagating at the superlens interfaces, in addition to scattered fields from the object. It is the coupling of these surface waves, which originate from higher spatial frequency waves scattered by the object, i.e. evanescent waves, that resonantly enhances them resulting in amplitudes that contribute to the image domain. These fields can be superimposed on the image fields in the space where we need to make measurements, making it more difficult to identify the true objects, see e.g.[9]. For this specific simulation, these artifacts are diminished when the objects are placed closer together (Figure 2(b)) and/or the objects have longer dimensions along the y-direction (Figure 2(c)). In general larger lens dimensions and finer computational meshes, combined with perfectly matched boundary layers are to be preferred. In addition, the artifacts are also suppressed if the superlens has higher losses (Figure 2(d)). However, this rather defeats the purpose of using a negative index lens, since when we allow the losses to increase we lose the resolution advantage of using the lens in the first place.
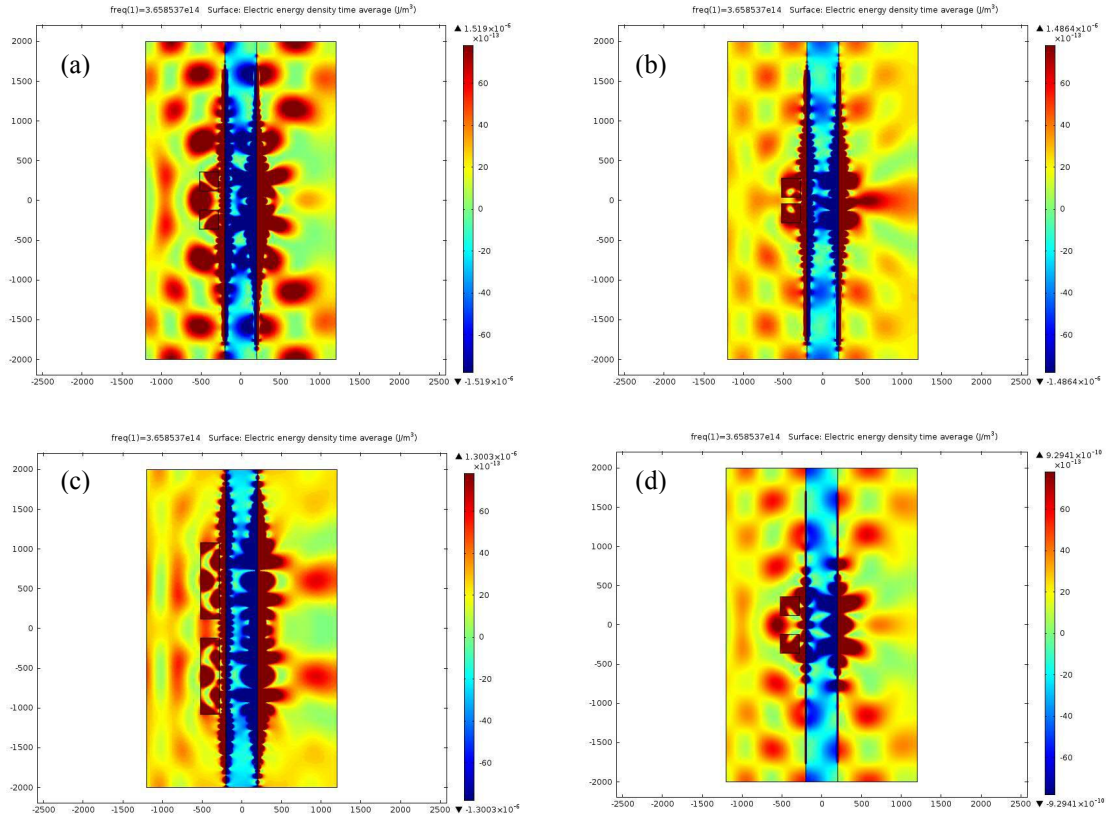
Figure 2. Interference patterns under different conditions (a) a chosen example (λ=820 nm; w=240 nm; d=240 nm; ε_{lens}= -1-5*$10^{-5}i$) (b) objects are placed closer together (d=80 nm) (c) objects have a longer dimension in the y-direction (w=720 nm) (d) the superlens has higher loss (ε_{lens}= -1-$10^{-2}i$)

3. MATHEMATICAL MODELS AND FILTERING TECHNIQUES

We consider a penetrable scattering object, $V(\mathbf{r})$ in a homogeneous background of permittivity ε_0; the object is related to the permittivity by $V(\mathbf{r}) = k^2[\varepsilon(\mathbf{r}) - 1]$, assuming ε_0=1. The scattered field $\Psi_s(\mathbf{r}, k\hat{\mathbf{r}}_0)$, due to the interaction of incident wave $\Psi_0(\mathbf{r}, k\hat{\mathbf{r}}_0)$ with the object $V(\mathbf{r})$, can be expressed in two dimensions by the integral equation

$$\Psi_s(\mathbf{r}, k\hat{\mathbf{r}}_0) = \frac{\exp(ikr)}{\sqrt{8\pi kr}} \int_D d^2r' \, V(\mathbf{r}')\Psi(\mathbf{r}, k\hat{\mathbf{r}}_0)\exp(-ik\hat{\mathbf{r}}\mathbf{r}') \tag{1}$$

where $\mathbf{r}_0$ denotes the incident field direction. The solution to this equation to find $V(\mathbf{r})$ requires the knowledge of total field $\Psi(\mathbf{r}, k\hat{\mathbf{r}}_0)$ within the object volume D, which is clearly not possible when $V(\mathbf{r})$ is unknown. For an object classified as a weak scatterer, i.e. that the first Born approximation is valid then a necessary condition is that the product of target's permittivity, its characteristic dimension, a, and wave number, k, should be much less than unity [6]. This is expressed mathematically as $kVa \ll 1$ where V is some measure of the maximum value that $V(\mathbf{r}) = \varepsilon(\mathbf{r}) - 1$ takes. If this assumption is reasonable, then the total field $\Psi(\mathbf{r}, k\hat{\mathbf{r}}_0)$ in the integral can be replaced by the known incident field $\Psi_0(\mathbf{r}, k\hat{\mathbf{r}}_0)$. For the special case of a plane wave incident, this linearizes the inversion problem and permits one to find a

solution, since the integral in equation (1) reduces to a Fourier transform between the scattered field data $\Psi_s\left(\mathbf{r}, k\hat{\mathbf{r}}_0\right)$ and $V(\mathbf{r})$. When imaging, including evanescent waves for which $k > k_0$, the field pattern in the image domain will represent the product of $V(\mathbf{r})$ with the total field, bandlimited by the transfer function of the superlens. In practice, at optical frequencies we are unable to follow the phase of the field and so we measure a quantity given by the time averaged Poynting vector. In the simulations presented here, we primarily show the electric time averaged energy density but it is also informative to observe the properties of the electromagnetic field.

3.1 Simple averaging: $<\Psi_{\text{transferred}}(\lambda,x,y)> \sim <\Psi_{\text{total}}(\lambda,x,y)>$

If we assume that we have a perfect lens, then we assume that the information in the object domain can be perfectly transferred to the image domain. The total field along a chosen plane in the image domain should be identical to the total field at a corresponding plane in the object domain. Practically, we cannot measure the total fields in the object domain. In a simulation, this can give us the ideal baseline for judging image resolution and quality. Given the fluctuations in the field, we consider combining image fields resulting from using several (slightly) different wavelengths. We can form $<\Psi_{\text{transferred}}(\lambda,x,y)> \sim <\Psi_{\text{total}}(\lambda,x,y)>$, where $\Psi_{\text{total}}(\lambda,x,y)$ is the total field (including incident field and the scattered field) in the object domain and $\Psi_{\text{transferred}}(\lambda,x,y)$ is the total field at the corresponding plane in the image domain, following modification by the lens transfer function. Figure 3 shows the simple averaging results of three chosen wavelengths (720 nm, 730 nm, 740 nm) and five chosen wavelengths (710 nm, 720 nm, 730 nm, 740 nm, 750 nm), but we are not seeing as good an estimate of $V(x,y)$ as we would like.
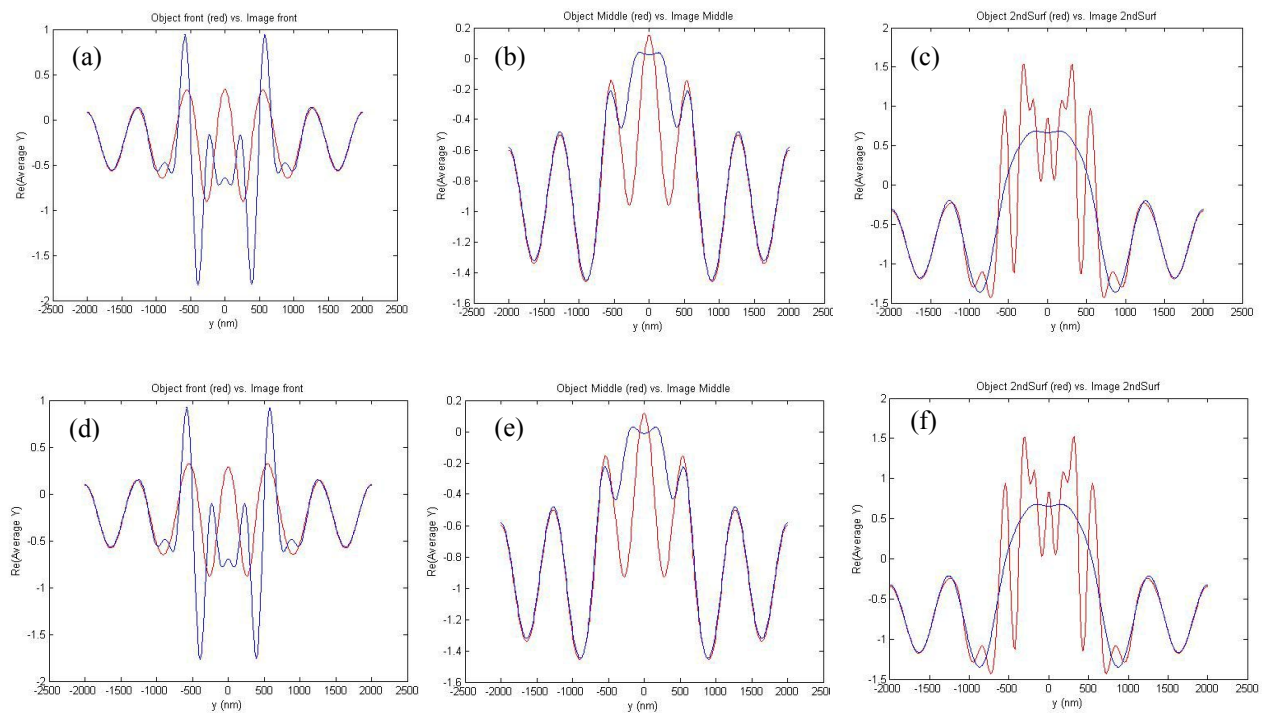

Figure 3: $<\Psi_{\text{transferred}}(\lambda,x,y)>$ and $<\Psi_{\text{total}}(\lambda,x,y)>$ at different chosen planes (a~c) λ=720 nm, 730 nm, and 740 nm (d~f) λ=710 nm,720 nm, 730 nm, 740 nm, and 750 nm. Red curves are in the object domain and blue in the image domain.

3.2 The weakly scattering case: $\Psi_{total}(\lambda,x,y) \sim V(x,y)*\Psi_{inc}(\lambda,x,y)$

If we assume the first Born approximation applies, then $\Psi_{total}(\lambda,x,y) \sim V(x,y)* \Psi_{inc}(\lambda,x,y)$, where $\Psi_{inc}(\lambda,x,y)$ is the incident field, in a perfect imaging system,

$$\Psi_{transferred}(\lambda,x,y)= \Psi_{total}(\lambda,x,y) \sim V(x,y)* \Psi_{inc}(\lambda,x,y) \tag{2}$$

The multiplicative relationship can be linearized for more effective averaging, if we apply a logarithm to equation (2), which gives

$$\ln(\Psi_{transferred}(\lambda,x,y))\sim\ln(|V(x,y)|)+\ln(|\Psi_{inc}(\lambda,x,y)|)+\text{i}*[\arg(V(x,y))+\arg(\Psi_{inc}(\lambda,x,y))] \tag{3}$$

If we further assume that $V(x,y)$ is a real positive number (i.e. $\ln(|V(x,y)|)= \ln(V(x,y))$ and $\arg(V(x,y))=0$) and if the incident field is a plane wave with $|\Psi_{inc}(\lambda,x,y)|=1$,

$$\ln(V(x,y))\sim \text{Re}\{\ln(\Psi_{transferred}(\lambda,x,y))\} \tag{4}$$

where Re{.} denotes taking the real part. Therefore, we could get the average of $\text{Re}\{\ln(\Psi_{transferred}(\lambda,x,y))\}$ from using different incident wavelengths to perhaps provide a better estimate of $\ln(V(x,y))$ and then calculate $V(x,y)$ by taking the exponential of $\ln(V(x,y))$. Thus:

$$V(x,y)=\exp\{\ln(V(x,y))\}\sim \exp\{<[\text{Re}(\ln(\Psi_{transferred} (\lambda_m,x,y)))]>\},\ m=1,2,3\ldots\text{etc.} \tag{5}$$

Here, we only consider three wavelengths (720 nm, 730 nm, and 740 nm) and $\varepsilon_{lens}= -1-10^{-2}i$. In practice, the wavelength range of a metamaterial supporting $n \sim -1$ is likely to be quite small, but we wish to demonstrate here whether the idea is sound.
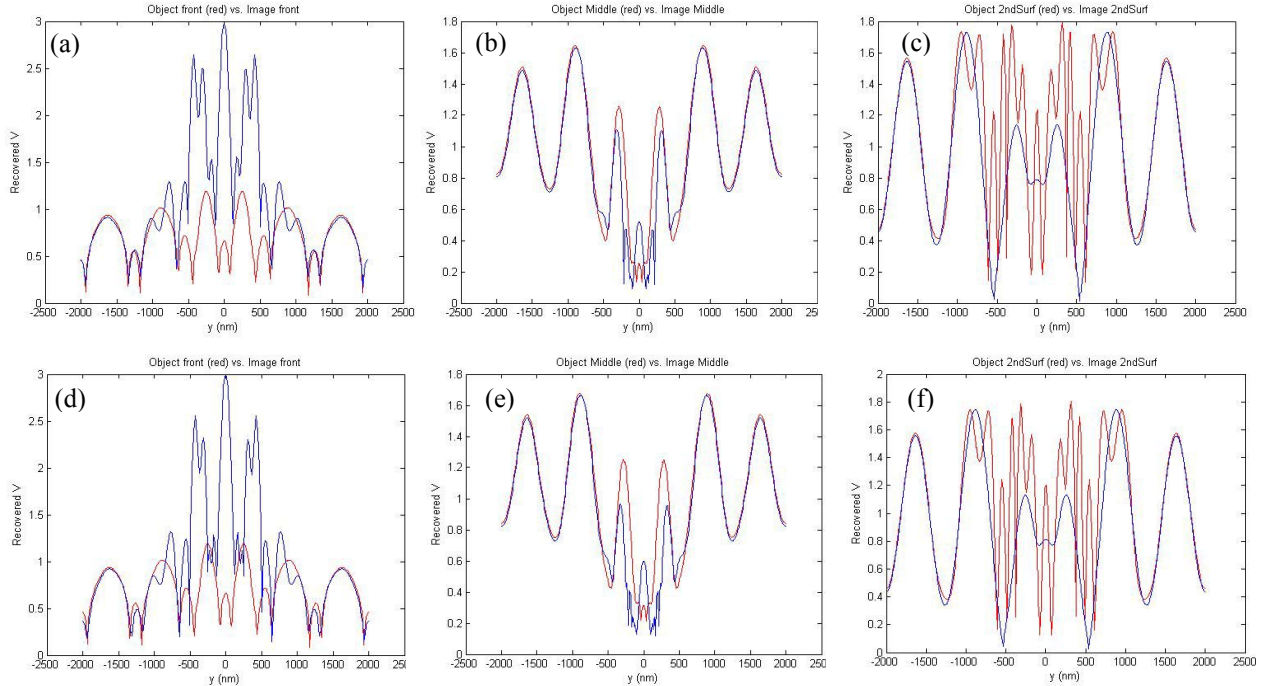

Figure 4 Calculated $V(x,y)$ calculated using equation (5) at different chosen planes (same data set as in Figure 3)
(a~c) λ=720 nm, 730 nm, and 740 nm (d~f) λ=710 nm,720 nm, 730 nm, 740 nm, and 750 nm.

These results, based on adopting a simple inverse scattering / nonlinear processing step to improve the averaging of several images, by taking the logarithm of the field, are disappointing. One can clearly see that the large field fluctuations arising from evanescent fields, that are contributing to higher resolution, are dominating at different locations in the object domain but are doing so in a complementary fashion in the image domain. If we increase the number of the incident wavelengths included in the calculation (Figure 4(d~f)), the recovered $V(x,y)$ in the image domain does not seems to match better with the one in the object domain (Figure 4(e)), indicating the choice of incident wavelengths for solving the inverse problem could be critical in identifying the object profile .

We note that the first Born approximation assumed here is usually interpreted physically to mean single scattering rather than multiple scattering events occur. Thus for higher spatial frequencies, and hence the associated evanescent waves, multiple scattering will make this approximation increasingly poor.

Based on equation (3)

$$Im(ln(\Psi_{transferred}(\lambda,x,y))) \sim Im(ln(\Psi_{total}(\lambda,x,y))) \sim arg(\Psi_{inc}(\lambda,x,y)) \qquad (6)$$

Figure 5 show $Im(ln(\Psi_{transferred}(\lambda,x,y)))$ and $Im(ln(\Psi_{total}(\lambda,x,y)))$ at different chosen planes under different wavelengths of illumination. If the total field and the perfect transferred field can be described by the first Born approximation (eq. (2)), the two curves in each plot in Figure 5 should be coincident (=$arg(\Psi_{inc})$). These results imply that the simple relation described in equation (2) is incomplete since it does not include the influence from the surface waves and the interference effects due to the boundary conditions. However, the phase plots in the middle planes (i.e. x=-400 nm and x=400 nm) clearly indicate the location of the objects. The middle phases in both the object and image domains, do seem to correlate with the wavefront delays introduced by the objects; this tells us some useful information is being transferred through the lens, but since we cannot measure phase, we need to find a solution to extract it from intensity measurements.
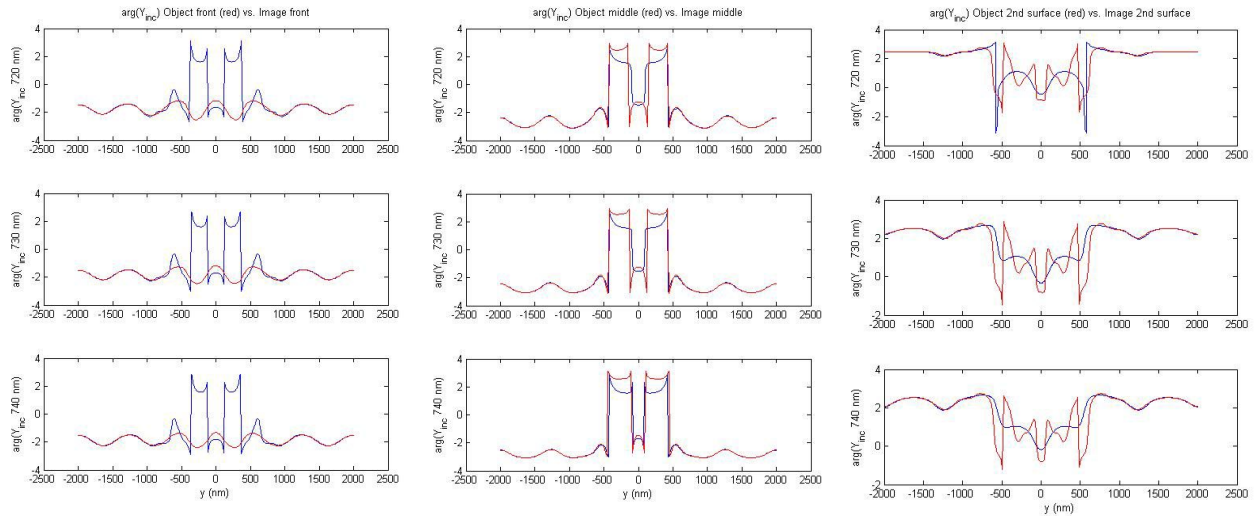

Figure 5 $Im(ln(\Psi_{transferred}(\lambda,x,y)))$ and $Im(ln(\Psi_{total}(\lambda,x,y)))$ at different chosen object-image planes for different illumination wavelengths.

3.3 $1+V\Psi$

In some cases where $|\Psi_{transferred}(\lambda,x,y)| < 1$, the logarithm become very large and negative which would amplify arguments with values less than unity, especially those close to zero. To investigate the importance of avoiding this concern, we let

$$1+\Psi_{transferred}(\lambda,x,y)\sim 1+ V(x,y)*\Psi_{inc}(\lambda,x,y) \cong V'(x,y)*\Psi_{inc}(\lambda,x,y) >1 \tag{7}$$

and we write

$$\text{Re}(1+\Psi_{transferred}(\lambda,x,y))\sim\text{Re}(\ln(V'(x,y)*\Psi_{inc}(\lambda,x,y))) = \ln(V'(x,y)) \tag{8}$$

Hence

$$\ln(V'(x,y)) \sim <\text{Re}(\ln(1+\Psi_{transferred}(\lambda_m,x,y))>, m=1,2,3\ldots\text{etc.} \tag{9}$$

$$V'(x,y) \sim \exp(<\text{Re}(\ln(1+\Psi_{transferred}(\lambda_m,x,y)))>), m=1,2,3\ldots\text{etc.} \tag{10}$$

and

$$V(x,y)= [V'(x,y)*\Psi_{inc}(\lambda,x,y)-1]/\Psi_{inc}(\lambda,x,y) \tag{11}$$

$$V(x,y) = <(V'(x,y)*\Psi_{inc}(\lambda_m,x,y)-1)/\Psi_{inc}(\lambda_m,x,y)>, m=1,2,3\ldots\text{etc.} \tag{12}$$

Using this, the recovered $V'(x,y)$ are displayed in Figure 6 at different chosen planes.
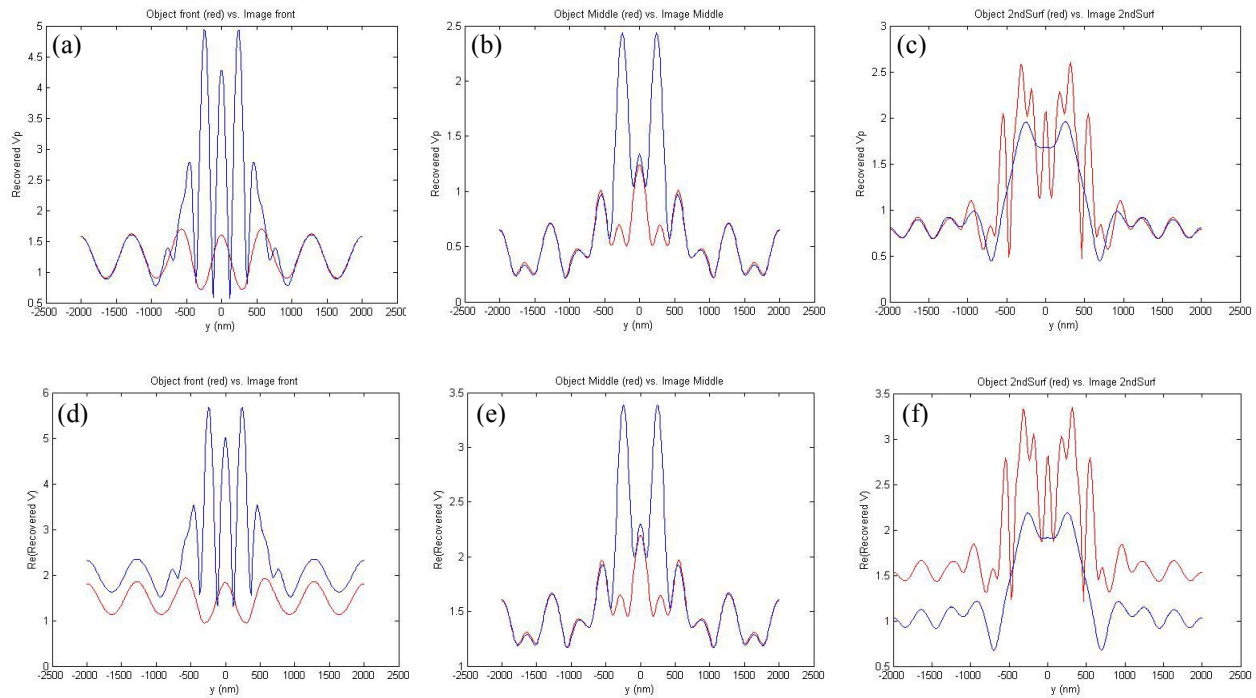

Figure 6 Calculated (a~c) $V'(x,y)$ and (d~f) $V(x,y)$ based on equation (9) and equation (11) respectively at different chosen planes

3.4 $\Psi_{total}(\lambda,x,y) \sim \Sigma(V(x,y)*\Psi_{inc}(\lambda_m,x,y))$ and similarly, $\Psi_{total}(\lambda,x,y) \sim <(V(x,y)*\Psi_{inc}(\lambda_m,x,y))>$

We consider the following condition and assume,

$$\Psi_{transferred}(\lambda,x,y)= \Psi_{total}(\lambda,x,y) \sim \Sigma(V(x,y)* \Psi_{inc}(\lambda_m,x,y))= V(x,y)* \Sigma (\Psi_{inc}(\lambda_m,x,y)), m=1,2,3\ldots etc. \tag{13}$$

$$\ln(\Psi_{transferred}(\lambda,x,y))\sim\ln(V(x,y))+\ln(|\Sigma (\Psi_{inc}(\lambda_m,x,y))|)+i*\arg(\Sigma (\Psi_{inc}(\lambda,x,y))) , m=1,2,3\ldots etc. \tag{14}$$

$$Re(\ln(\Psi_{transferred}(\lambda,x,y)))\sim \ln(V(x,y))+\ln(|\Sigma (\Psi_{inc}(\lambda_m,x,y))|) , m=1,2,3\ldots etc. \tag{15}$$

then

$$\ln(V(x,y)) \sim <\{Re(\ln(\Psi_{transferred}(\lambda_m,x,y)))\}> - \ln(|\Sigma (\Psi_{inc}(\lambda_m,x,y))|), m=1,2,3\ldots etc. \tag{16}$$

$$V(x,y) \sim \exp(<\{Re(\ln(\Psi_{transferred}(\lambda_m,x,y)))\}> - \ln(|\Sigma (\Psi_{inc}(\lambda_m,x,y))|)), m=1,2,3\ldots etc. \tag{17}$$

$$V(x,y) \sim \exp(<\{Re(\ln(\Psi_{transferred}(\lambda_m,x,y)))\}>) / | \Sigma (\Psi_{inc}(\lambda_m,x,y))|, m=1,2,3\ldots etc. \tag{18}$$

Similarly, if

$$\Psi_{transferred}(\lambda,x,y)= \Psi_{total}(\lambda,x,y) \sim <(V(x,y)* \Psi_{inc}(\lambda_m,x,y))>, m=1,2,3\ldots etc. \tag{19}$$

$$Re(\ln(\Psi_{transferred}(\lambda,x,y)))\sim \ln(V(x,y))+\ln(|\Sigma (\Psi_{inc}(\lambda_m,x,y))|) - \ln(m) , m=1,2,3\ldots etc. \tag{20}$$

then

$$\ln(V(x,y)) \sim <\{Re(\ln(\Psi_{transferred}(\lambda_m,x,y)))\}> - \ln(|\Sigma (\Psi_{inc}(\lambda_m,x,y))|) + \ln(m) , m=1,2,3\ldots etc. \tag{21}$$

$$V(x,y) \sim \exp(<\{Re(\ln(\Psi_{transferred}(\lambda_m,x,y)))\}>) / |sum(\Psi_{inc}(\lambda_m,x,y))|*m, \; m=1,2,3\ldots etc. \tag{22}$$

The recovered $V(x,y)$ based on equation (18) and equation (21) should present the same trend as the one based on equation (4) shown in Figure 4 except for a ratio of $| \Sigma (\Psi_{inc}(\lambda_m,x,y))|^{-1}$ and $| \Sigma (\Psi_{inc}(\lambda_m,x,y))|^{-1}*m$ respectively. Unfortunately, neither approach revealed any improvement.

CONCLUSIONS

The motivation for this paper is that we seek to image information about a scattering object on a sub-wavelength scale, ideally better than ~ $\lambda/5$ to make it worth the effort. We also want to be able to image penetrable objects, which by their very nature are assumed to have interesting sub-wavelength-scale small features. These structures will multiply scatter and generate evanescent waves, some of which may be transformed into propagating waves. This mix of propagating and evanescent waves is transferred through an ideal negative one lens which in practice will be bandlimited by the metamaterial's micro-structure. Evanescent waves generated from scattering features that are closer to the lens surface will be more efficiently captured and transferred by the lens, but will necessarily create high amplitude fields in the image plane between the lens face and the associated image focal plane. Also, the observed fields in the image domain require some wavelength or angle diversity in order to successfully apply an inverse scattering algorithm and thereby separate the superresolved permittivity profile we want from the complex field patterns that are measured. We note that at optical frequencies we can only measure intensity, while inversion algorithms generally require information about both the amplitude and the phase of the scattered radiation. One approach to this so-called "phase problem" is to provide a reference wave and gather intensity measurements from interference patterns, i.e. perform holography. It may be possible in the context of negative index slab superresolution imaging that we can contrive to image objects that have some known scattering reference point adjacent to the object under inspection. With this a priori knowledge, one might be able to better characterize the (desirable) surface-wave patterns associated with the lens and remove them by further processing, to better reveal an image of the entire V or $V\Psi$ at high resolution, rather than just features originating close to the front face of the slab lens.

More important than this, is that we have identified a fundamental paradox to superresolved imaging using a slab negative index lens. For higher resolution we need lower loss metamaterials which in turn will create much larger

amplitude evanescent waves representing those higher spatial frequencies. Clearly, the higher the spatial frequency, the faster its decay in the propagation distance x, i.e. they decay as exp ($- k_y* $ x). There is a fundamental trade-off here, since the wider the object in the propagation direction, the more these huge amplitude decaying exponentials associated with features in the object closest to the lens will increasingly mask the image of those parts of the object further from the lens. In practice, it appears unavoidable that we have to accept an infinitessimally thin image plane at some x, if we want to have arbitrarily high resolution. Similarly, if we have an object wider than $\sim \lambda/2$, there is little expectation that high spatial frequency evanescent waves from features far from the surface of the lens, and that would be needed in the image domain, will even make it to the lens at all. Thus this trade-off suggests a simple figure of merit exists relating object dimensions to image resolution. The concept of the number of degrees of freedom for an optical system provides some guidance [10]. The number of degrees of freedom is given by $\{A \, \Delta n / (\lambda^2)\}$ in 2D, where A is the area of the object and Δn some measure of the object's maximum refractive index (i.e. square root of the permittivity). In 2D for example, if the object has area X*Y and we choose the resolution we want to be λ /M in the x direction and if $\{A \, \Delta n / (\lambda^2)\} =$ constant, then improving the resolution in Y by a factor of M necessarily requires that we degrade resolution in X by the same factor.

ACKNOWLEDGMENTS

REFERENCES

[1]   M. E. Testorf and M. A. Fiddy, "Superresolution Imaging: Revisited", Advances in Imaging and Electron Physics, Ed. P. W. Hawkes, Vol 163, ch 5, pp166-218, Ed. P. W. Hawkes, Academic Press, (2010).

[2]   J. B. Pendry, "Negative index makes a perfect lens", Phys. Rev. Lett., 85, 18, pp 3966-3969 , 2000.

[3]   Z. Jacob et al, "Optical hyperlens: far field imaging beyond the diffraction limit", Optics Express, 14, 18, pp 8247-8256, 2006.

[4]   E. Wolf, "Three-dimensional structure determination of semi-transparent objects from holographic data," *Optics Comm.*, 1, 1969.

[5]   X-X Liu and A. Alu, "Limitations and potentials of metamaterial lenses", J. of Nanophotonics, Vol 5, 053509-1-13, 2011.

[6]   Yuan Zhang, Yi-Chen Chuang and M. A. Fiddy, "Study of scattering patterns and sub-wavelength scale imaging based on finite-sized metamaterials", Applied Physics A DOI 10.1007/s00339-01106738-9, (2011)

[7]   Yi-Chen Chuang, R. Dudley and M. A. Fiddy, "Optimal arrangement of meta-atoms composing metamaterials", SPIE Paper 8269   82691D1-7, Photonic and Phononic Properties of Engineered Nanotructures II, Ed. A.Adibi, S-Y Lin and A. Scherer, Photonics West January 2012.

[8]   C. P. Moore et al, "An improved transfer-matrix model for optical superlenses", Optics Express 17, no 16, pp14260-14269, 2009.

[9]   R. Hegde et al, "The dynamics of nanoscale superresolution imaging with the superlens", IEEE MTT 59, 10 pp 2612- 2623, 2011.

[10]   R. S. Ritter and M. A. Fiddy, "Imaging from scattered fields: limited data and degrees of freedom ", SPIE Paper 8500-6, Image Recovery from Incomplete Data VII, Ed. P.J. Bones, M. A. Fiddy and R. Millane, August 2012.